Dual Electronic and Optical Monitoring of Biointerfaces by a Grating-Structured Coplanar-Gated Field-Effect Transistor

Roger Hasler, Pietro A. Livio, Anil Bozdogan, Stefan Fossati, Simone Hageneder, Verónica Montes-García, Jacopo Movilli, Taghi Moazzenzade, Luna Loohuis, Ciril Reiner-Rozman, Adrián Tamayo, Christine Fiedler, Maria Ibáñez, Christoph Kleber, Jurriaan Huskens, Jakub Dostalek, Paolo Samorì, and Wolfgang Knoll

***Abstract*—We present a novel, portable sensor platform that enables concurrent monitoring of surface mass and charge density variations at thin biointerfaces. This platform combines a coplanar-gated field-effect transistor (FET) architecture with grating-coupled surface plasmon resonance (SPR), yielding an integrated disposable sensor chip prepared by nanoimprint and maskless photolithography techniques. The sensor chip design is suitable for scalable production and relies on reduced graphene oxide (rGO), serving as the FET's semiconductor material for the electronic readout, and a metallic gate electrode surface that is corrugated with a multidiffractive structure for optical probing with resonantly excited surface plasmons (SPs). Together with its integration in a compact instrumentation, this results in a form factor optimized solution for dual-mode investigations without compromising the optical or electronic sensor performance. A poly-L-lysine (PLL)-based thin linker layer was deployed at the sensor surface to covalently attach azide-conjugated biomolecules by using incorporated "clickable" dibenzocyclooctyne (DBCO) moieties. Interestingly, the dual-mode measurements allow elucidating the role of the globular nature of the PLL chains when increasing the density of DBCO attached to their backbone, leading to PLL folding and internalization of DBCO moieties, and thus reducing the coupling yield for the used deoxyribonucleic acid (DNA) oligomers. We envision that this platform can be employed to studying a range of other biointerface architectures and biomolecular interaction phenomena, which are inherently tied to mass and charge density variations.**

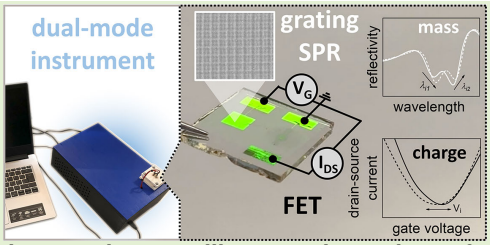

***Index Terms*— Click chemistry, coplanar-gated field-effect transistor (FET), dual-mode sensing, grating-surface plasmon resonance (SPR), poly-L-lysine (PLL).**

Received 13 December 2024; revised 13 January 2025; accepted 13 January 2025. Date of publication 29 January 2025; date of current version 2 April 2025. This work was supported in part by European Union's Horizon 2020 Research and Innovation Programme—BORGES under Marie Skłodowska-Curie Grant 813863; in part by the Federal Government of Lower Austria, K3-Group—Culture, Science, and Education through the Project "Responsive Wound Dressing;" in part by the Gesellschaft für Forschungsförderung (GFF) of Lower Austria under Project FTI22-G-012; in part by Austrian Research Promotion Agency (FFG), within the COMET Project "PI-SENS," under Project 915477; and in part by the Federal Provinces of Lower Austria and Tirol. The work of Anil Bozdogan was supported by Austrian Science Fund (FWF) under Grant P 35103-B. The work of Stefan Fossati and Jakub Dostalek were supported in part by Czech Science Fund through the Project APLOMA under Grant 22-30456J; in part by the Operational Programme Johannes Amos Comenius financed by European Structural and Investment Funds; and in part by Czech Ministry of Education, Youth, and Sports, under Project SENDISO-CZ.02.01.01/00/22_008/0004596. The work of Simone Hageneder and Jakub Dostalek were supported by FWF under Project DIPLAB I 5119-B. The work of Jurriaan Huskens was supported by Netherlands Organization for Scientific Research (NWO) under TOP Grant 715.015.001. The associate editor coordinating the review of this article and approving it for publication was Dr. Barbara Adinolfi. *(Corresponding author: Roger Hasler.)*

Please see the Acknowledgment section of this article for the author affiliations.

This article has supplementary downloadable material available at https://doi.org/10.1109/JSEN.2025.3533113, provided by the authors.

Digital Object Identifier 10.1109/JSEN.2025.3533113

I. Introduction

BIOANALYTICAL methods for monitoring biomolecular interactions at solid–liquid interfaces are essential for investigating various biological phenomena and developing new technologies in healthcare and diagnostics [1], [2]. Among these methods, surface plasmon resonance (SPR) biosensors are routinely used for the label-free monitoring of biomolecular affinity interactions by measuring respective refractive index changes occurring on a metallic sensor surface [3]. More specifically, this is done by probing the surface of the sensor in real time with excited surface plasmon (SP) waves, allowing changes in surface mass density of affinity-bound biomolecules within the SP evanescent field penetrating to a distance of about 100 nm to be quantified. This label-free method allows for reliable analysis of large- and medium-sized biomolecules, but for low molecular weight analytes or biomolecular systems undergoing conformation changes it needs to be combined with other approaches, including but not limited to, for example, labeling with fluorescent or nanoparticle tags [4], [5].

Electrolyte-gated field-effect transistors (EG-FETs) have become an established bioanalytical platform for detecting chemical and biological species, as well as biomolecular

interactions, in a way that complements SPR biosensors [6]. This is because beyond changes in surface mass density, most biomolecular surface interactions also involve variations in surface charge. EG-FETs are three-terminal devices in which the current through a semiconductor channel is modulated by a gate voltage (V_G), creating an electrical double layer (EDL) at the interface, which is highly sensitive to changes in surface charge density from attached molecules. This results in a label-free, low-voltage sensor that is stable in aqueous environments and with high sensitivity to interactions with low molecular weight molecules occurring within close proximity to the sensor surface, typically below 10 nm [7], [8].

Recently, the combination of SPR with electronic readouts on EG-FETs has drawn increasing attention for simultaneous, label-free surface interrogation [9]. Integrating SPR on the EG-FET gate electrode allows for concurrent characterization of surface functionalization, analyte binding, and sensor response calibration [10]. Real-time monitoring of both optical and electronic signals allows for the deconvolution of mass and charge uptake and charge redistribution in multilayer assemblies [11]. However, this approach is constrained by bulky optical components and impractical nonplanar gate architectures. A more practical solution would be a single disposable sensor chip that integrates both transduction principles. Alternative SPR methods beyond attenuated total reflection (ATR) have been explored, such as using metallic nanostructures for localized SPs [12] or diffraction gratings for propagating SPs [13]. Additionally, SPR readout using periodic nanohole arrays have been integrated into planar electrochemical sensors [14], though this approach requires optical probing through the analyte medium and depends on redox-active species, which limit its range of applications.

Herein, we report a novel sensor system based on grating-structured coplanar-gated field-effect transistors (FETs), which enables simultaneous optical and electronic readout on the gate surface. Optical readout is achieved through backside excitation of propagating SPs using multiperiodic gratings (MPGs), which were fabricated by mass-production compatible nanoimprint lithography [15], [16]. We investigate how MPGs impact FET fabrication on glass substrates, evaluate device performance, and compare it to the top-gated FET/SPR platform based on ATR with Kretschmann geometry. As a proof of concept, devices were functionalized with a poly-L-lysine (PLL) biointerface modified with dibenzocyclooctyne (DBCO) for orthogonal and covalent functionalization with an azide-modified deoxyribonucleic acid (DNA) oligomer through strain-mediated click chemistry. This functionalization was monitored optically and electronically, offering insights into linker conformation, density, and binding site accessibility.

II. Experimental Section

A. Fabrication of Grating-Structured Coplanar-Gated FET Substrates

A schematic representation of the fabrication steps is shown in Fig. 1. Details of the MPG structure that was developed by Hageneder et al. [15] using UV-laser interference lithography (UV-LIL) can be found in previous work. Polydimethylsiloxane (PDMS) stamps, based on the optimized grating, were used to fabricate the grating-structured FET substrates. BK7 glass substrates (1 mm thick) were cut to 1.5 × 1.5 cm and cleaned by sonication in a 1% Hellmanex[1] III aqueous solution for 15 min, then Milli-Q grade DI-H_2O for 15 min, and finally ethanol for 15 min, before blow-drying with compressed air. They were then coated with Amonil MMS 10 via spin coating (3000 r/min, 120 s), resulting in an Amonil layer of ≈110 nm. The PDMS stamp was then placed on top of the Amonil layer to imprint the grating structure. Trapped air was allowed to escape for 5 min at room temperature (RT), followed by UV curing at 365 nm with a dose of 2 J·cm^{-2} (UV lamp Bio-Link 365, Vilber Lourmat).

FETs with interdigitated electrode (IDE) architecture (see Fig. S1) (six pairs, 30/30 μm electrode/gap, $W/L = 266$, and channel size $A_{ch} = 0.24$ mm^2) and a coplanar gate electrode (3 × 3 mm, $A_g = 9$ mm^2) were fabricated using maskless photolithography and lift-off on top of the grating structured substrate as previously reported [17]. The gate-to-channel size ratio is ∼38 with a gate-channel distance of 4 mm. In brief, the grating-structured substrates were sonicated in isopropanol for 5 min, blow-dried with N_2, and then heated on a hot plate at 140 °C for 3 min. They were cooled to RT under a flow of N_2, spin-coated with AZ1505 photoresist (3000 r/min, 45 s) and placed on a hot plate at 100 °C for 1 min. The FET architecture was patterned by photolithography at 405 nm and 238 mJ·cm^{-2} using a Microtech LW405B laser writer. The irradiated parts of the AZ1505 layer were developed in AZ726 MIF developer for 10 s, washed with Milli-Q grade DI-H_2O, and blow-dried with N_2. A 60 nm gold layer was deposited by thermal evaporation (Plassys MEB 300 with 2 × 10^{-7} mbar at 0.3 Å·s^{-1}), followed by lift-off of the sacrificial photoresist via sonication in acetone for 5 min. The resulting substrates were washed with isopropanol and blow-dried with N_2. The reduced graphene oxide (rGO) channel on top of the IDEs was prepared according to previous reports [17]. The IDEs were prefunctionalized with poly(diallyldimethylammonium chloride) (PDADMAC) as an electrostatic anchor layer for graphene oxide (GO) deposition which was then electrochemically reduced (further details see Supplementary Information).

B. Dual-Mode Setup

Substrates were connected to a Keithley 4200-SCS probe station with spring-loaded gold pins (see Fig. S20). A PDMS reaction chamber with a clearance hole was filled with phosphate buffered saline (PBS) electrolyte and the transfer characteristics ($I_{DS}V_G$ curves) measured. Therefore, V_G was swept from −0.8 to 0.8 V (200 mV·s^{-1}) with a constant drain–source voltage of $V_{DS} = 50$ mV, measuring the drain–source current (I_{DS}) and gate- or leakage current (I_G).

Optical measurements were achieved via a Y-fiber optic (FO) splitter (400 μm core diameter, Thorlabs Inc.), integrated into the bottom of the sample holder. The substrate was placed on the holder with the backside in direct contact with the end-face of the fiber coupler, positioned below the gate electrode (see Supplementary Information). Polychromatic light (halogen, 12 V, HL-2000-LL, Ocean Insight) was directed

[1]Trademarked.

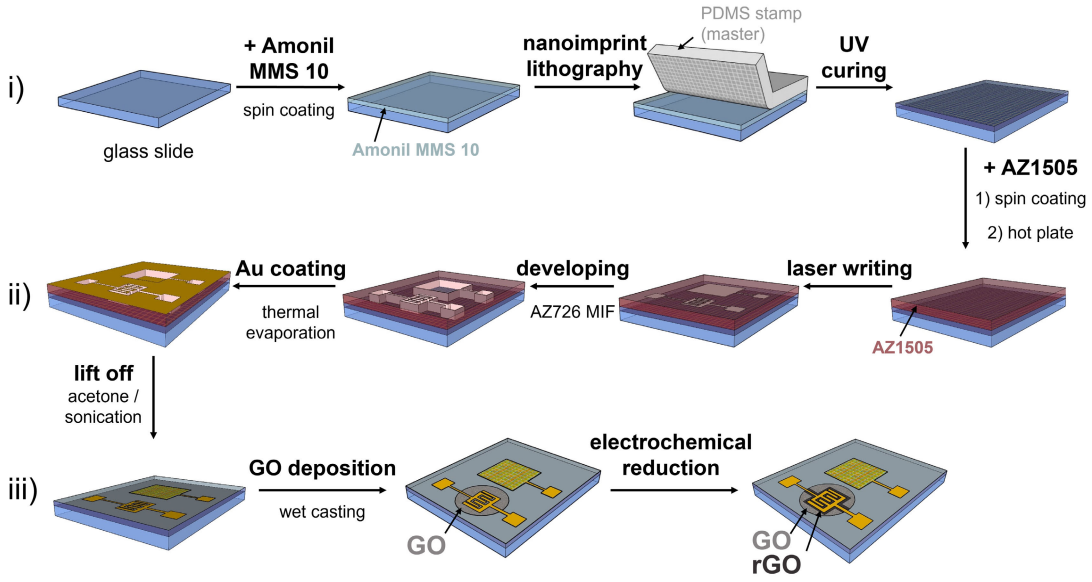

Fig. 1. Schematic representation of the fabrication steps involved in the preparation of the grating-structured coplanar-gated FET device including i) imprinting of the nanostructure (optical signal), ii) fabrication of the FET architecture (electronic signal), and iii) deposition of the transistor channel material.

to the backside of the substrate through the Y-splitter. The reflected beam from the MPG structure was routed to a spectrometer (HR4000, Ocean Insight), with spectra normalized against a reference flat gold surface. The normalized reflectivity spectra were processed by a dedicated LabView software, developed in-house.

C. Biomolecular Binding Study

The rGO channel and the gate electrode were functionalized with PLL-oligo(ethylene glycol) (OEG)-DBCO. Initial optical and electronic signals were recorded in PBS 1X. Nuclease-free PBS 1X was used for all biomolecular binding studies. The sensor surface was coated with a polymer monolayer using a PLL-OEG-DBCO solution in PBS (0.5 mg·mL^{-1}) for 1 h, as reported [18]. The substrates were then rinsed with PBS, after which the optical and electronic signals were recorded in PBS. Additionally, an azide-modified DNA oligomer based on a previously reported structure [19] was clicked to the DBCO-moieties of the PLL layer via strain-promoted alkyne-azide cycloaddition. For this, a 1 μM azide-DNA oligomer solution in PBS with 1 mM $MgCl_2$ was applied for 1 h, followed by rinsing. Optical and electronic signals were then recorded after oligomer functionalization in PBS.

III. Results and Discussion

A. Sensor Chip Preparation

Dual-mode sensing was integrated into a coplanar-gated FET/SPR device using sensor chips with MPG corrugation, fabricated through a facile process (see Fig. 1). An example of the sensor chip is shown in Fig. 2(a), with a detailed scanning electron microscopy (SEM) image of the imprinted MPG in Fig. 2(b). Combining coplanar FET architecture with an MPG structure integrates both transducing principles on a single chip, simplifying fabrication and enabling flexible device design [17]. Notably, the preparation process relies solely on industrial-compatible nano- and micro-fabrication techniques, paving the way for future mass production of FET/SPR devices without the need for complex lithography.

The FET devices were successfully fabricated on MPG-structured glass substrates, similar to those on standard glass (see Fig. S2). The resulting gold electrode edges on the grating-structured substrates showed slight impairments, likely due to the nanoimprint resist (which covers the entire substrate) interfering with the sacrificial photoresist and/or gold layer during the lift-off process. However, the electronic functionality of the electrodes was intact, allowing MPG-structured devices to function as FETs.

rGO was used as the semiconductor due to its ambipolar behavior, which allows for the discrimination of cation and anion density changes under varying gate potentials, an essential feature for a platform designed to study affinity-driven biomolecular interactions. GO was electrostatically anchored, using PDADMAC as polycationic adhesive primer and electrochemically reduced in bi-distilled water, aligning with a fully green and scalable device fabrication (see Figs. S3 and S4 of Supplementary Information,). The rGO-based FET channel was characterized using SEM and Raman spectroscopy, which confirmed a homogenous and successfully reduced rGO film (see Supplementary Information). Comparison to standard glass slides showed that the MPG structure did not negatively affect the rGO channel fabrication (see Fig. S5). Raman mapping revealed that the film predominantly consists of more than five rGO layers, with no significant differences between devices with and without MPG structure (see Section C of Supplementary Information).

B. Dual-Mode Sensor Platform

The FET/SPR sensor chip was placed in the sample holder with a PDMS reaction chamber clamped onto the surface, confining the electrolyte (see Figs. 2(c) and S20). Electronic connectivity was established through three spring-loaded pins

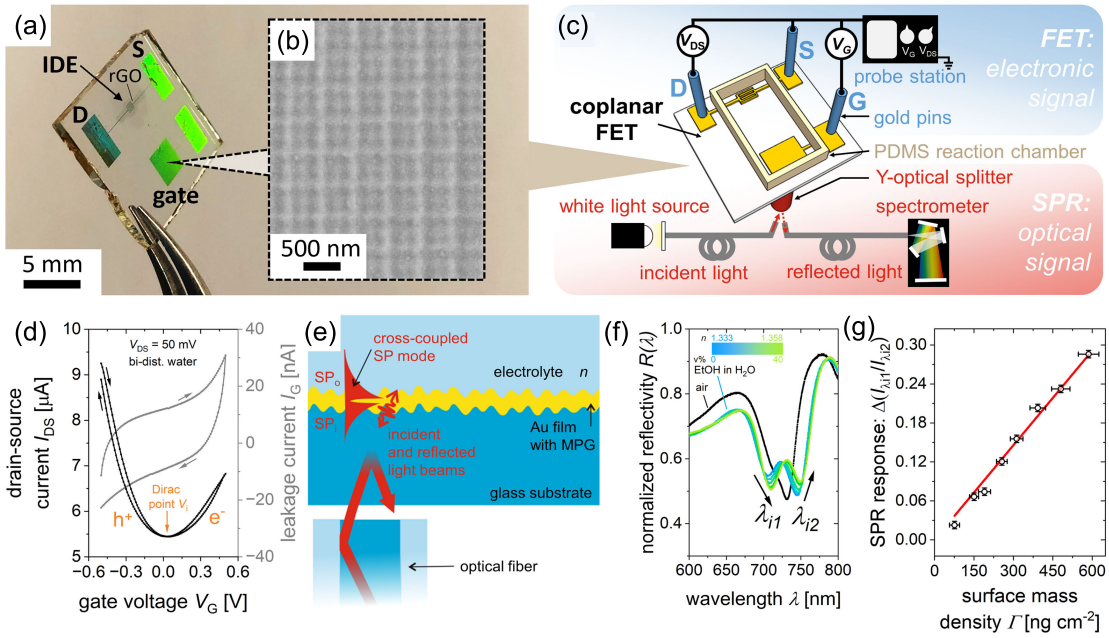

Fig. 2. (a) Photographic image of the device, with (b) SEM image of the grating structured gate electrode. (c) Schematic representation of the dual mode setup. (d) Electronic signal (I_{DS} V_G, black), indicating hole (h^+) and electron (e^-) accumulation branch, and the Dirac point (V_i). Leakage current (I_G) is shown in gray. Arrows indicate the V_G scan direction. (e) Schematic representation of the coupling to the optical signal via backside excitation. (f) Optical signal obtained from different ethanol/water dilutions. (g) SPR calibration of the intensity ratio shift with adsorbed surface mass density and the linear fit (red).

that made contact with the source, drain, and gate pad on the chip, which were then connected to the measurement unit. Optical signals were recorded simply by irradiating the backside of the chip with polychromatic light coupled to a Y-FO splitter connected to a portable UV/visible (VIS) spectrometer. The key advantage of the MPG structure is that it enables direct optical probing in reflection mode, with the optical beam impinging from the substrate side, unlike conventional grating-coupled SPRs. This design enables facile operation and allows for the convenient exchange of electrolyte and analyte solutions from the top of the chip. Furthermore, this setup also facilitates flow cell integration and simplifies user handling. The developed compact instrumentation, integrating all necessary auxiliary hardware, is shown in Section F of Supplementary Information. Compared to other FET/SPR platforms, it does not require complex or expensive optical components and no moving parts or special environmental requirements (for example, system encapsulation or alignment).

C. Electronic Signal Characterization

The electronic signal transduction is based on the I_{DS} modulation upon application of V_G. The effective modulation via V_G results from binding events at the MPG gate electrode (38 times larger than the rGO channel), induced by the electric field effect and capacitive coupling. $I_{DS}V_G$ transfer and $I_{DS}V_{DS}$ output characteristics were recorded to assess the electronic performance. It has previously been demonstrated that EG-FET technology can be transferred to a coplanar gate arrangement without compromising the device's performance [17]. Typical ambipolar $I_{DS}V_G$ transfer curves were obtained, with a hole (h^+) and electron (e^-) accumulation branch and the minimum of the transfer curve being denoted as Dirac point (V_i) [see Fig. 2(d)]. No significant dependence on the distance between gate electrode and channel was observed (see Section D of Supplementary Information), as expected based on previous studies in top-gated configuration [10]. I_G was two orders of magnitude lower than I_{DS}, with no redox peaks, indicating electrochemical stability, proper gating with functional isolation and negligible parasitic effects. Additionally, linear $I_{DS}V_{DS}$ curves showed no issues with contact resistance up to 200 mV V_{DS} with V_G from -500 to 500 mV (see Fig. S9). The applied V_{DS} of 50 mV in this study is well within the linear regime. Despite the slight electrode edge impairment, fabricated devices show stable and repeatable operation (see Fig. S10) and no significant impact on the electronic performance due to the presence of the MPG was observed (see Fig. S11). The performance was consistent with devices on standard Si/SiO_2 wafers with the same IDE geometry [17]. Therefore, we conclude that the MPG structure does not significantly alter the measured electronic signals.

D. Optical Signal Characterization

The MPG structure, which carries the thin gold film acting as the gate electrode, enables resonant excitation of SPs, providing complementary optical readout. The MPG features two superimposed periodic corrugations with periods of $\Lambda_1 = 456$ nm and $\Lambda_2 = 240$ nm, determined by fast Fourier transformation (FFT) analysis of atomic force microscopy (AFM) topography (see Fig. S13). These periods align closely with the original pattern prepared by UV-LIL [15], validating the imprinting process. The resulting structure enables SPs

diffraction excitation on the same area as the gate electrode [see Fig. 2(e)] (layer deposition and adhesion details are in the Supplementary Information, Figs. S14–S16). The optical backside excitation mechanism enabled by cross-coupling of SP modes from the inner (SP_i) and outer (SP_o) side of the gold film is schematically shown in Fig. 2(e). It relies on the designed MPG corrugation components facilitating 1st-order diffraction-based phase matching of the incident beam traveling in the far-field with SP_i mode (component Λ_1) at the inner interface followed by the transfer of electromagnetic field intensity through the Au film to the SP_o mode, which propagates along the outer interface in opposite direction (component Λ_2) via their evanescent field tails [15].

Reflectivity spectra from the MPG gate electrode [see Fig. 2(f)] exhibit two superimposed Lorentzian dips at distinct wavelengths of λ_{i1} and λ_{i2}. These two dips occur due to the diffraction coupling of counter-propagating SP_i and SP_o modes that lead to the splitting of their dispersion relation as previously discussed [15], [16]. Fig. 2(f) shows two reflectivity dips that exhibit a small red-shift with increasing n (from 1.33 to 1.36 for ethanol in water). The coupling strength ($I_{\lambda i1}$) increases for the lower wavelength dip (λ_{i1}), while the coupling strength ($I_{\lambda i2}$) decreases for the longer wavelength component (λ_{i2}). The SPR response was defined as the intensity ratio $I_{\lambda i1}/I_{\lambda i2}$ (see Fig. S17), yielding a bulk refractive index sensitivity $S_B = \Delta(I_{\lambda i1}/I_{\lambda i2})/\Delta n_o$ of 14 ± 1 RIU^{-1} and resolution of $(4.4 \pm 0.7) \times 10^{-5}$ RIU from a calibration step (see Fig. S18). To convert the SPR response to the surface mass density, a calibration using layer-by-layer (LbL) deposition of oppositely charged PEMs was performed (details see Supplementary Information) [16]. Linear fitting yielded a correlation of $(4.9 \pm 0.1) \times 10^{-4}$ $cm^2 \cdot ng^{-1}$ ($R^2 = 0.997$) [see Fig. 2(g)].

E. Dual-Mode Sensor Operation

The large SPR surface/gate compared to the FET channel size ensures high capacitance at the gate/electrolyte interface, forming a larger EDL and allowing the electric field to be more strongly influenced by surface mass and charge at the SPR interface. This results in stronger signal coupling at the SPR interface compared to the channel, promoting both spatial and temporal concurrence.

To validate dual-mode operation, the sensor was tested with electrolytes of increasing ionic strength (H_2O, PBS 0.1X, and PBS 1X) (see Supplementary Information). Minor reflectivity changes, corresponding to a slight increase in bulk refractive index, were observed, while significant shifts in the $I_{DS}V_G$ transfer curves confirmed sensitivity to ionic strength. The Dirac point shift and steeper e^- and h^+ accumulation branch slopes aligned with previous findings, indicating responsiveness to ionic environments [20], [21]. The marked difference in the magnitude of optical and electronic signals underscores the benefit of combining these two transducing principles, as the electronic response is particularly valuable for detecting small changes for example in ionic concentration or pH due to charge redistributions at the solid–liquid interface [11]. Interestingly, the asymmetric FET responses to ionic strength, more prominently affecting the e^- accumulation branch, resemble the signals observed when increasing gate size (see Fig. S22), suggesting that the FET response is primarily influenced by changes at the gate/electrolyte (capacitance) interface. Furthermore, a more symmetric shift of the $I_{DS}V_G$ curve is expected with diminishing influence of gate surface effects [10], [20].

The impact of V_G on the optical signal has been explored in plasmonic fiber gate electrodes with an FET [10], and similar effects were observed for the MPG-structured coplanar gate. Here, optical signal reversibility and short regeneration times after the V_G bias application were noted (Fig. S23, discussion in Supplementary Information). Both signal channels delivered stable responses without requiring thermal pretreatment, unlike fiber optic gates [22]. Dual-mode operation remained effective, with stable optical signals after V_G cycling (for transfer curves) or during constant V_G application (for real-time electronic sensing), which minimizes SPR cross-sensitivity.

F. Surface Functionalization

There are various methods for preparing biointerfaces and attaching receptor units to optical and electronic biosensors [6], [23], which often involve linker molecules designed for specific surfaces, such as thiol derivatives for gold [24] or pyrene linkers for graphene-based substrates [25]. To enhance the versatility of the sensor platform and avoid these surface-specific limitations, we used a surface modification strategy based on physisorption of functionalized polyelectrolytes (PLL-OEG-DBCO) [18]. This approach enables uniform deployment on both the rGO channel and the gold gate electrode [see Fig. 3(a)].

The amine groups of lysine side chains in PLL are positively charged at physiological pH, facilitating adsorption onto negatively charged surfaces through electrostatic interactions. PLL and its derivatives adsorb quickly and efficiently across a wide range of surfaces, including silicon dioxide [18], gold [18], [26], various metal oxides [27], [28], polymers [29], and graphene [30]. Despite its versatility, PLL has rarely been used in electronic devices [30], [31], [32], [33]. PLL derivatives, with "clickable" moieties, allow for covalent postfunctionalization with diverse molecules, such as proteins or antibodies, enhancing specificity for various analytes [33]. For instance, azide-modified biomolecules can be bound to the DBCO groups of the PLL interface [18], [26] through strain-promoted alkyne-azide cycloaddition, allowing precise receptor density control [34]. Additionally, the OEG side chains in PLL provide antifouling properties, minimizing nonspecific protein adsorption [35], [36].

To confirm similar adsorption of PLL-OEG-DBCO on rGO and Au surfaces, it was initially immobilized on functionalized FO-SPR substrates (details in Supplementary Information). Rapid adsorption with similar binding kinetics was observed on both surfaces (see Figs. 3(b) and S21). Subsequently, an azide-modified DNA oligomer ("N_3-DNA"), which specifically binds to interleukin 6 (an inflammatory response protein), was clicked onto the interface. This DNA oligomer sequence, based on a previously reported aptamer probe [19], has demonstrated effectiveness in detecting interleukin 6 in prior studies [37], [38], [39]. Comparable quantities of adsorbed PLL-$OEG_{29.4\%}$-$DBCO_{6.6\%}$ and DNA oligomer were immobilized on

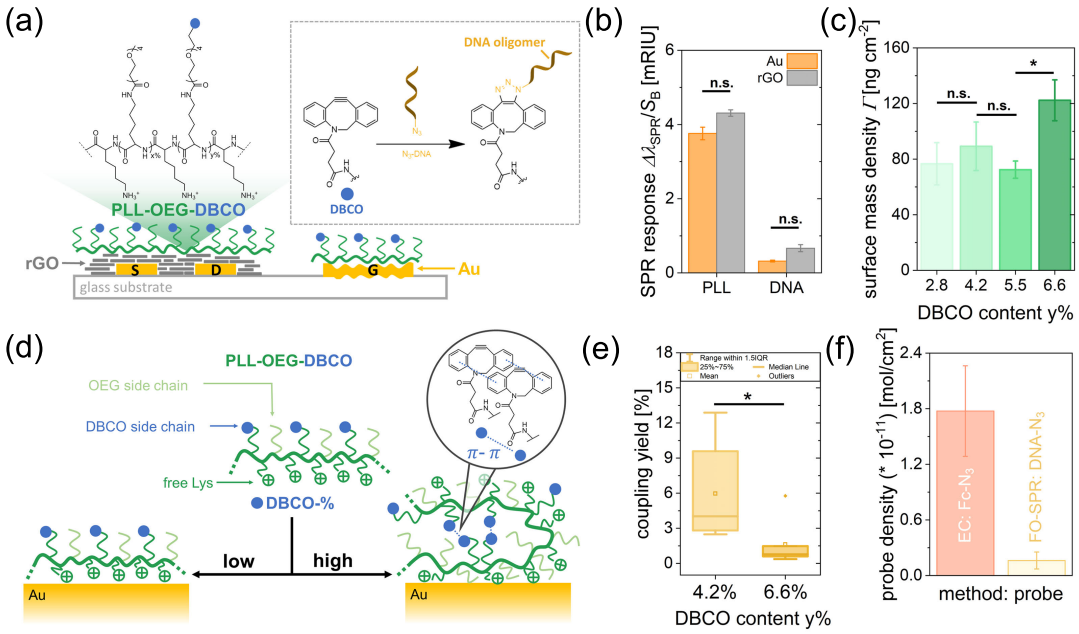

Fig. 3. (a) Schematic representation of the PLL surface functionalization with click-modification using a N_3-DNA oligomer (box). (b) FO-SPR signals for adsorbed PLL (6.6% DBCO) and attached N_3-DNA on Au and rGO, respectively ($n = 3$). (c) Surface mass densities for immobilized PLL-OEG-DBCO on gold depending on the degree of DBCO side chain functionalization ($n = 3$). (d) Schematic representation of the PLL interface with low or high DBCO content. (e) Coupling yield of the DNA oligomer to the immobilized PLL-OEG-DBCO layer depending on the degree of DBCO side chain modifications ($n = 6$). (f) Probe density attached to PLL (with 4.2% DBCO), determined electrochemically (EC) with N_3-Fc and via FO-SPR with N_3-DNA. Pairwise ANOVA analysis was performed for (b), (c), and (e) and statistically significant differences indicated ($* p < 0.05$, n.s. = no significance).

both Au and rGO surfaces [see Fig. 3(c)], with rGO showing slightly higher signals due to its higher amount of negative surface charge from residual oxygen-containing groups. Statistical analysis, however, showed no significant difference between the two surfaces, enabling functionalization with a controlled degree of covalently attached receptors on either the gate, the channel, or both. This approach also offers an alternative to electrochemical functionalization of graphene with "clickable" aryl diazonium species, achieving functionalization without modifying graphene's electronic properties [40].

To investigate how varying DBCO content in PLL affects the functionalization process, PLL compounds (see Table S1 of Supplementary Information) with increasing DBCO content of $y = 2.8\%$, 4.2%, 5.5%, and 6.6% were immobilized on SPR substrates. Results indicated that higher DBCO content led to an increase in surface mass density, with 122 ± 15 ng·cm^{-2} for PLL containing 6.6% DBCO, compared to 79 ± 16 ng·cm^{-2} in average for PLL compounds with lower DBCO content [see Fig. 3(c)]. This suggests that higher DBCO content alters the PLL interface, potentially due to π–π stacking interactions between DBCO groups on the PLL backbone. In solution, these intramolecular interactions were indicated by the broadening of the DBCO peak in the ^{1}H NMR spectra (see Figs. S28–S32). The absence of aggregates, confirmed by dynamic light scattering (DLS) (see Fig. S33), suggests that intermolecular interactions are unlikely due to the positive charge of PLL. The intramolecular interaction of DBCO should lead to a globular structure of PLL chains with their DBCO groups incorporated in their interior [see Fig. 3(d)]. The surface adsorption leads to thicker PLL layers as for other PLL derivatives [34], confirming that the globular nature is conserved upon immobilization, resulting in higher surface mass density. This was also confirmed by quartz crystal microbalance (QCM), showing greater frequency shifts and increased dissipation for PLL with higher DBCO content (see Fig. S34).

However, at higher DBCO content (above 5%), the conformational change of the PLL chains leads to a lower coupling yield for subsequent click reactions with DNA oligomers (see Fig. 3(e)], likely due to a reduced number of available DBCO groups. The click functionalization of the PLL interface (with 4.2% DBCO) was validated using an azide-modified redox probe ("Fc–N_3") (see Supplementary Information). Redox peaks, observed only for the DBCO-containing PLL interface, indicate surface-bound behavior and a probe density of $1.8 \pm 0.5 \times 10^{-11}$ mol·cm^{-2}, consistent with previously reported values [see Fig. 3(f)] [26]. The lower probe density for the azide-modified DNA oligomer ($0.2 \pm 0.1 \times 10^{-11}$ mol·cm^{-2}), measured via FO-SPR (calculation in Supplementary Information), can be attributed to increased steric and electrostatic repulsion between DNA oligomers [see Fig. 3(f)]. Despite the reduced coupling yield, the dilution of recognition units may be advantageous for sensing applications by minimizing repulsive interactions (steric and/or electrostatic) between adsorbed species [41].

G. Multimodal Biointerface Investigation

The PLL-DNA biointerface, with its significant differences in mass and charge between PLL and DNA, was used to assess the dual-mode sensor chip's ability to distinguish these

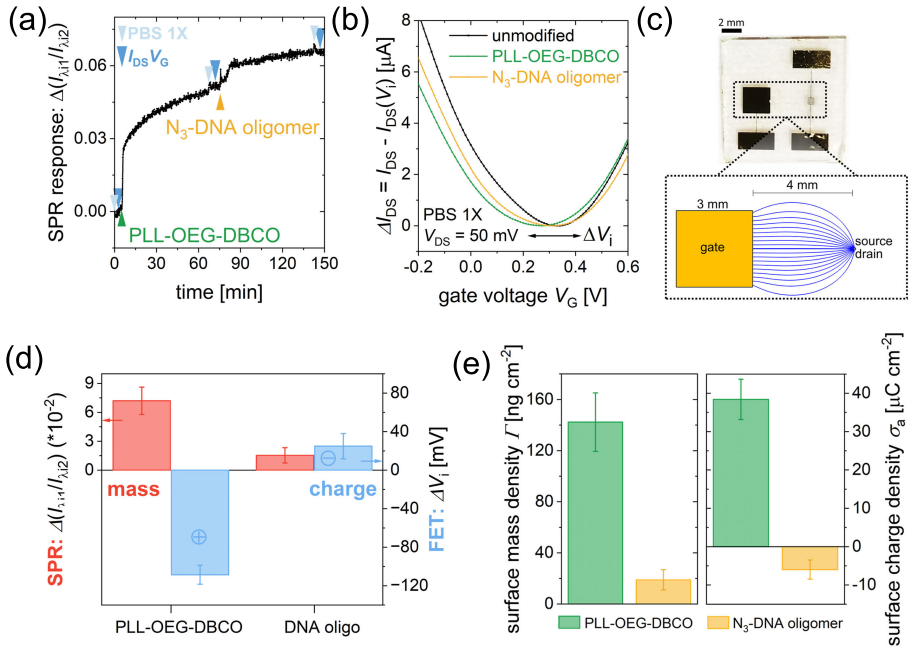

Fig. 4. Dual-mode investigation of the PLL-DNA biointerface using PLL with 6.6% DBCO. (a) In situ SPR readout for PLL coating and subsequent click-functionalization with the N_3-DNA oligomer. (b) I_{DS} V_G curves of unmodified devices, after PLL coating and DNA oligomer click functionalization, in PBS 1X and with $V_{DS} = 50$ mV. (c) Image of the FET geometry and an illustration of the resulting electric field lines. (d) Evaluated optical response (red bars) and electronic response (Dirac point shifts, blue bars) for the two functionalization steps ($n = 3$). (e) Surface mass (left) and surface charge density (right) quantification based on the optical readout.

differences. As a proof-of-principle, both the gate and channel were functionalized with PLL-OEG$_{29.4\%}$-DBCO$_{6.6\%}$ and then clicked with the N_3-DNA oligomer. Note that, for a biosensor, functionalization of only the gate would be advantageous to omit any rGO signals. However, the gate functionalization was in situ monitored via grating-coupled SPR [see Fig. 4(a)]. The SPR signal revealed rapid electrostatic adsorption of PLL-OEG-DBCO, followed by DNA oligomer binding, confirming gate functionalization. The observed refractive index change indicated mass uptake on the sensor surface [3] [see Fig. 4(d)]. The dense monolayer of PLL-OEG-DBCO caused a more significant intensity ratio shift compared to the lighter, sparsely attached DNA oligomer (≈11 kDa), which was controlled by DBCO side chain density.

Simultaneously, $I_{DS}V_G$ transfer curves were recorded before and after each functionalization step [see Fig. 4(a)], sweeping V_G from −800 to 800 mV in PBS 1X. Fig. 4(b) shows a detailed view of the measured I_{DS}, normalized by the current at the Dirac point ($I_{DS(Vi)}$). The I_{DS} is modulated according to the equation

$$I_{DS} = (W/L) \cdot C_i \cdot \mu \cdot (V_G - V_T) \cdot V_{DS} \quad (1)$$

where W is the channel width, L the channel length, C_i the effective capacitance per unit area, μ the charge mobility, and V_T the threshold voltage. The large gate-to-channel area ratio of ∼38, makes the gate function as the working electrode. This is attributed to the higher gate capacitance and the higher field density at the FET channel [see Fig. 4(c)]. The larger gate surface area allows for greater mass and charge adsorption, which displaces the electric field more effectively than adsorption at the smaller FET channel, resulting in a stronger impact on I_{DS}. The potential changes at both the gate-electrolyte and channel-electrolyte interfaces alter the transconductance $|g_m|$ decreasing from 17.1 μS for the unmodified sensor, to 12.3 μS after PLL-OEG-DBCO addition, and 12.5 μS for N_3-DNA oligomer immobilization (evaluated for the e^- accumulation branch). Hence, the biolayer formation reduces the slopes of the e^- and h^+ accumulation branches (see Fig. S39). The formation of the dense PLL monolayer is also indicated in the measured leakage current and a detailed discussion can be found in Section M of Supplementary Information. Additionally, the functionalization also caused significant Dirac point shifts, linked to the differing charges of the immobilized species [see Fig. 4(d)]. The PLL-OEG$_{29.4\%}$-DBCO$_{6.6\%}$ is positively charged due to the protonated amino groups of the lysine side chains at physiological pH and led to a negative shift of $\Delta V_i = -109 \pm 10$ mV. This behavior aligns with expectations, as a positively charged target leads to a depletion of hole carriers in the rGO [42], while exerting capacitive effects, a trend similarly observed in PLL-modified graphene [30]. These results are consistent with findings from top-gated FET devices, using a planar Kretschmann-SPR configuration (see Fig. S36). No significant dependency of ΔV_i on the DBCO content in PLL was observed (see Fig. S37). The measured ΔV_i correlates with the quantity of unfunctionalized lysine in the various PLL-OEG-DBCO compounds (see Fig. S37), supporting the fact that the increase in optical density with higher DBCO content is due to intramolecular rearrangement of DBCO side chains rather than the intermolecular PLL agglomerations. Otherwise, an increase in surface charge density from free lysine groups would be expected. Binding of the negatively charged DNA oligomer subsequently caused a

positive shift of $\Delta V_i = 25 \pm 13$ mV, only partially offsetting the positive charge from the PLL layer. This shift had no significant effect on transconductance, suggesting minimal capacitive coupling from oligomer binding. The dual mode-sensing platform's strength is underscored here, as the positive surface charge shift, crucial for characterizing biomolecular layer properties, would remain undetected by SPR alone.

The grating-SPR response quantified the surface mass density as 142 ± 23 ng·cm^{-2} for PLL-OEG$_{29.4\%}$-DBCO$_{6.6\%}$ and 19 ± 8 ng·cm^{-2} for the DNA oligomer [see Fig. 4(e)], aligning with results from FO-SPR and planar Kretschmann-SPR configurations. This optical readout on the gate electrode allows for precise interpretation of the electronic signals based on ΔV_i and $\Delta|g_m|$. Specifically, the sign of ΔV_i reveals the type of surface charge immobilized, while the surface mass density provides a basis for calculating of the exact amount adsorbed (see Supplementary Information). The adsorbed surface charge densities were determined to be σ_a of 38 ± 5 and -6 ± 3 μC·cm^{-2} for the PLL-OEG$_{29.4\%}$-DBCO$_{6.6\%}$ and the DNA oligomer, respectively [see Fig. 4(e)], consistent with the ratio from the corresponding ΔV_i values. This supports the observed low coupling yield due to intramolecular interactions among the DBCO groups (see Supplementary Information). Comparing the optical and electronic signals highlights the dual-mode platform's complementary insights [see Fig. 4(d)]. It is important to note that this quantification of the adsorbed interfacial charge is not directly measurable via the FET signal alone due to overlapping influences of the interfacial capacitor and charge transfer resistor (see Supplementary Information). Integrating grating-coupled SPR onto a coplanar FET gate creates a facile and versatile platform, capable of simultaneously tracking surface binding events, identifying the type of charge involved, and quantifying both surface mass and charge density.

IV. Conclusion

We developed an innovative multimodal sensor platform that combines grating-coupled SPR and a coplanar-gated FET on a single chip, providing simultaneous monitoring of surface mass and charge density variations. For surface functionalization, we demonstrate DBCO-modified PLL with covalent conjugation of an azide-modified DNA oligomer as an effective approach for graphene (electronic) and gold (optical) biointerface engineering. This platform also allows for comparative studies on the effects of selective functionalization at either the gate or the channel.

With a compact FET design, simplified optical readout for grating-coupled SPR, and the seamless integration of these components, this sensor chip offers substantial benefits over traditional FET/SPR systems [10], [11]. Additionally, the industrial compatible manufacturing process supports scalability, paving the way for future multiplexing and parallel multichannel detection. Together with its integration in a compact instrumentation provides an optimized solution for dual-mode surface investigations without compromising the optical or electronic sensor performance compared to other FET/SPR platforms (see Table S2). Furthermore, adjusting the MPG periods allows to tune the working wavelength depending on the application in mind which is not straightforward for the other configurations. The versatile biointerface architecture shared by the optical and electronic sensor enhances this dual-mode sensor platform for multiparameter analysis, supporting advanced investigations into biomolecular interactions at the solid–liquid interface and thus guides further biosensor developments based on organic electronics.

Acknowledgment

The authors would like to thank the Electron Microscopy Facility at ISTA for their support with sputter coating the FO probes and NOSI GmbH for their support with 3-D printing.

Roger Hasler and Wolfgang Knoll are with the AIT Austrian Institute of Technology GmbH, 3430 Tulln, Austria, and also with the Laboratory for Life Sciences and Technology (LiST), Faculty of Medicine and Dentistry, Danube Private University, 3500 Krems an der Donau, Austria (e-mail: roger.hasler@dp-uni.ac.at; wolfgang.knoll@dp-uni.ac.at).

Pietro A. Livio, Verónica Montes-García, Adrián Tamayo, and Paolo Samorì are with the Institut de Science et d'Ingénierie Supramoléculaires, Université de Strasbourg, CNRS, 67000 Strasbourg, France.

Anil Bozdogan is with the AIT Austrian Institute of Technology GmbH, 3430 Tulln, Austria, and also with the Division of Clinical Virology, Medical University of Vienna, 1090 Vienna, Austria.

Stefan Fossati is with the AIT Austrian Institute of Technology GmbH, 3430 Tulln, Austria, and also with the FZU-Institute of Physics, Czech Academy of Sciences, 182 21 Prague, Czech Republic.

Simone Hageneder is with the AIT Austrian Institute of Technology GmbH, 3430 Tulln, Austria.

Jacopo Movilli, Taghi Moazzenzade, Luna Loohuis, and Jurriaan Huskens are with the Department of Molecules and Materials, MESA+ Institute, Faculty of Science and Technology, University of Twente, 7500 AE Enschede, The Netherlands.

Ciril Reiner-Rozman and Christoph Kleber are with the Department of Chemistry and Physics of Materials, Faculty of Medicine and Dentistry, Danube Private University, 3500 Krems an der Donau, Austria.

Christine Fiedler and Maria Ibáñez are with the Institute of Science and Technology Austria (ISTA), 3400 Klosterneuburg, Austria.

Jakub Dostalek is with the AIT Austrian Institute of Technology GmbH, 3430 Tulln, Austria, also with the Laboratory for Life Sciences and Technology (LiST), Faculty of Medicine and Dentistry, Danube Private University, 3500 Krems an der Donau, Austria, and also with the FZU-Institute of Physics, Czech Academy of Sciences, 182 21 Prague, Czech Republic (e-mail: dostalek@fzu.cz).

Data Availability Statement

The data that support the findings of this study are openly available in Zenodo (10.5281/zenodo.10072667).

References

[1] J. Yao, M. Yang, and Y. Duan, "Chemistry, biology, and medicine of fluorescent nanomaterials and related systems: New insights into biosensing, bioimaging, genomics, diagnostics, and therapy," *Chem. Rev.*, vol. 114, no. 12, pp. 6130–6178, Jun. 2014.

[2] R. D'Agata, N. Bellassai, and G. Spoto, "Exploiting the design of surface plasmon resonance interfaces for better diagnostics: A perspective review," *Talanta*, vol. 266, Jan. 2024, Art. no. 125033.

[3] J. Homola, "Surface plasmon resonance sensors for detection of chemical and biological species," *Chem. Rev.*, vol. 108, no. 2, pp. 462–493, Feb. 2008.

[4] K. Sergelen et al., "Plasmon field-enhanced fluorescence energy transfer for hairpin aptamer assay readout," *ACS Sensors*, vol. 2, no. 7, pp. 916–923, Jul. 2017.

[5] A. Dillen, C. Scarpellini, W. Daenen, S. Driesen, P. Zijlstra, and J. Lammertyn, "Integrated signal amplification on a fiber optic SPR sensor using duplexed aptamers," *ACS Sens.*, vol. 8, no. 2, pp. 811–821, 2023.

[6] F. Torricelli et al., "Electrolyte-gated transistors for enhanced performance bioelectronics," *Nature Rev. Methods Primers*, vol. 1, no. 1, p. 66, Oct. 2021.

[7] E. Macchia et al., "Single-molecule detection with a millimeter-sized transistor," *Nature Commun.*, vol. 9, no. 1, p. 3223, 2018.

[8] N. Nakatsuka et al., "Aptamer-field-effect transistors overcome Debye length limitations for small-molecule sensing," *Science*, vol. 362, pp. 319–324, Oct. 2018.

[9] W. Knoll, J. Liu, F. Yu, L. Niu, C. Reiner-Rozman, and I. Köper, "Comparing surface plasmon-optical and electronic immuno-sensing of affinity interactions—A case study," *Chemosensors*, vol. 9, no. 1, p. 11, Jan. 2021.

[10] R. Hasler et al., "Field-effect transistor with a plasmonic fiber optic gate electrode as a multivariable biosensor device," *ACS Sensors*, vol. 7, no. 2, pp. 504–512, Feb. 2022.

[11] P. Aspermair et al., "Dual monitoring of surface reactions in real time by combined surface-plasmon resonance and field-effect transistor interrogation," *J. Amer. Chem. Soc.*, vol. 142, no. 27, pp. 11709–11716, Jul. 2020.

[12] B. Špačková, P. Wrobel, M. Bocková, and J. Homola, "Optical biosensors based on plasmonic nanostructures: A review," *Proc. IEEE*, vol. 104, no. 12, pp. 2380–2408, Dec. 2016.

[13] J. Dostálek, J. Homola, and M. Miler, "Rich information format surface plasmon resonance biosensor based on array of diffraction gratings," *Sens. Actuators B, Chem.*, vol. 107, no. 1, pp. 154–161, May 2005.

[14] K. Nakamoto, R. Kurita, and O. Niwa, "Electrochemical surface plasmon resonance measurement based on gold nanohole array fabricated by nanoimprinting technique," *Anal. Chem.*, vol. 84, no. 7, pp. 3187–3191, Apr. 2012.

[15] S. Hageneder, S. Fossati, N.-G. Ferrer, B. Güngörmez, S. K. Auer, and J. Dostalek, "Multi-diffractive grating for surface plasmon biosensors with direct back-side excitation," *Opt. Exp.*, vol. 28, no. 26, pp. 39770–39780, 2020.

[16] R. Hasler et al., "Surface plasmon resonance biosensor with anti-crossing modulation readout," *Sens. Actuators B, Chem.*, vol. 417, Oct. 2024, Art. no. 136163.

[17] R. F. de Oliveira et al., "Liquid-gated transistors based on reduced graphene oxide for flexible and wearable electronics," *Adv. Funct. Mater.*, vol. 29, no. 46, Nov. 2019, Art. no. 1905375.

[18] D. Di Iorio, A. Marti, S. Koeman, and J. Huskens, "Clickable poly-l-lysine for the formation of biorecognition surfaces," *RSC Adv.*, vol. 9, no. 61, pp. 35608–35613, 2019.

[19] K. L. Rhinehardt, S. A. Vance, R. V. Mohan, M. Sandros, and G. Srinivas, "Molecular modeling and SPRi investigations of interleukin 6 (IL6) protein and DNA aptamers," *J. Biomolecular Struct. Dyn.*, vol. 36, no. 8, pp. 1934–1947, Jun. 2018.

[20] I. Heller, S. Chatoor, J. Männik, M. A. G. Zevenbergen, C. Dekker, and S. G. Lemay, "Influence of electrolyte composition on liquid-gated carbon nanotube and graphene transistors," *J. Amer. Chem. Soc.*, vol. 132, no. 48, pp. 17149–17156, Dec. 2010.

[21] I. Heller, A. M. Janssens, J. Männik, E. D. Minot, S. G. Lemay, and C. Dekker, "Identifying the mechanism of biosensing with carbon nanotube transistors," *Nano Lett.*, vol. 8, no. 2, pp. 591–595, Feb. 2008.

[22] R. Hasler et al., "Optical and electronic signal stabilization of plasmonic fiber optic gate electrodes: Towards improved real-time dual-mode biosensing," *Frontiers Phys.*, vol. 11, Jul. 2023, Art. no. 1202132.

[23] K. Manoli et al., "Printable bioelectronics to investigate functional biological interfaces," *Angew. Chem. Int. Ed.*, vol. 54, no. 43, pp. 12562–12576, Oct. 2015.

[24] J. C. Love, L. A. Estroff, J. K. Kriebel, R. G. Nuzzo, and G. M. Whitesides, "Self-assembled monolayers of thiolates on metals as a form of nanotechnology," *Chem. Rev.*, vol. 105, no. 4, pp. 1103–1170, Apr. 2005.

[25] V. Georgakilas et al., "Noncovalent functionalization of graphene and graphene oxide for energy materials, biosensing, catalytic, and biomedical applications," *Chem. Rev.*, vol. 116, no. 9, pp. 5464–5519, May 2016.

[26] J. Movilli, R. W. Kolkman, A. Rozzi, R. Corradini, L. I. Segerink, and J. Huskens, "Increasing the sensitivity of electrochemical DNA detection by a micropillar-structured biosensing surface," *Langmuir*, vol. 36, no. 16, pp. 4272–4279, Apr. 2020.

[27] N.-P. Huang et al., "Poly(l-lysine)-g-poly(ethylene glycol) layers on metal oxide surfaces: Surface-analytical characterization and resistance to serum and fibrinogen adsorption," *Langmuir*, vol. 17, no. 2, pp. 489–498, Jan. 2001.

[28] G. L. Kenausis et al., "Poly(l-lysine)-g-poly(ethylene glycol) layers on metal oxide surfaces: Attachment mechanism and effects of polymer architecture on resistance to protein adsorption," *J. Phys. Chem. B*, vol. 104, no. 14, pp. 3298–3309, Apr. 2000.

[29] J. Movilli, D. Di Iorio, A. Rozzi, J. Hiltunen, R. Corradini, and J. Huskens, "'Plug-n-play' polymer substrates: Surface patterning with reactive-group-appended poly-l-lysine for biomolecule adhesion," *ACS Appl. Polym. Mater.*, vol. 1, no. 11, pp. 3165–3173, 2019.

[30] J. Gao et al., "Poly-l-lysine-modified graphene field-effect transistor biosensors for ultrasensitive breast cancer miRNAs and SARS-CoV-2 RNA detection," *Anal. Chem.*, vol. 94, no. 3, pp. 1626–1636, Jan. 2022.

[31] X. Duan et al., "Functionalized polyelectrolytes assembling on nano-BioFETs for biosensing applications," *Adv. Funct. Mater.*, vol. 25, no. 15, pp. 2279–2286, Apr. 2015.

[32] K. Li et al., "Ultrasensitive detection of exosomal miRNA with PMO-graphene quantum dots-functionalized field-effect transistor biosensor," *iScience*, vol. 25, no. 7, Jul. 2022, Art. no. 104522.

[33] G. E. Fenoy et al., "Interface engineering of 'clickable' organic electrochemical transistors toward biosensing devices," *ACS Appl. Mater. Interfaces*, vol. 15, no. 8, pp. 10885–10896, 2023.

[34] J. Movilli, A. Rozzi, R. Ricciardi, R. Corradini, and J. Huskens, "Control of probe density at DNA biosensor surfaces using poly(l-lysine) with appended reactive groups," *Bioconjugate Chem.*, vol. 29, no. 12, pp. 4110–4118, Dec. 2018.

[35] N.-P. Huang, J. Vörös, S. M. De Paul, M. Textor, and N. D. Spencer, "Biotin-derivatized poly(l-lysine)-g-poly(ethylene glycol): A novel polymeric interface for bioaffinity sensing," *Langmuir*, vol. 18, no. 1, pp. 220–230, Jan. 2002.

[36] S. Pasche, S. M. De Paul, J. Vörös, N. D. Spencer, and M. Textor, "Poly(l-lysine)-graft-poly(ethylene glycol) assembled monolayers on niobium oxide surfaces: A quantitative study of the influence of polymer interfacial architecture on resistance to protein adsorption by ToF-SIMS and in situ OWLS," *Langmuir*, vol. 19, no. 22, pp. 9216–9225, Oct. 2003.

[37] M. Muhammad, C.-S. Shao, and Q. Huang, "Aptamer-functionalized au nanoparticles array as the effective SERS biosensor for label-free detection of interleukin-6 in serum," *Sens. Actuators B, Chem.*, vol. 334, May 2021, Art. no. 129607.

[38] C. Diacci et al., "Organic electrochemical transistor aptasensor for Interleukin-6 detection," *ACS Appl. Mater. Interface*, vol. 16, no. 45, pp. 61467–61474, Nov. 2024, doi: 10.1021/acsami.3c12397.

[39] R. Hasler et al., "'Clickable' graphene nanoribbons for biosensor interfaces," *Nanosc. Horizons*, vol. 9, no. 4, pp. 598–608, 2024.

[40] V. Mishyn et al., "Controlled covalent functionalization of a graphene-channel of a field effect transistor as an ideal platform for (bio)sensing applications," *Nanosc. Horizons*, vol. 6, no. 10, pp. 819–829, 2021.

[41] P. A. M. Urbina et al., "Physical insights from the frumkin isotherm applied to electrolyte gated organic transistors as protein biosensors," *J. Mater. Chem. C*, vol. 9, no. 33, pp. 10965–10974, 2021.

[42] W. Fu, L. Jiang, E. P. van Geest, L. M. C. Lima, and G. F. Schneider, "Sensing at the surface of graphene field-effect transistors," *Adv. Mater.*, vol. 29, no. 6, Nov. 2016, Art. no. 1603610.